Songklanakarin J. Sci. Technol.
46 (2), 234–240, Mar. – Apr. 2024

http://www.sjst.psu.ac.th

Original Article

Metallurgy in railway turnout and rail flaw detection techniques♣

Thanapol Jirasukprasert[1], Manwika Kongpuang[1, 2*], Prapas Muangjunburee[1, 2], Nichapa Phrommahakul[1], and Suhaidee Sani[3]

[1] *Department of Mining and Materials Engineering, Faculty of Engineering, Prince of Songkla University, Hat Yai, Songkhla, 90110 Thailand*

[2] *Center of Excellence in Metal and Materials Engineering, Faculty of Engineering, Prince of Songkla University, Hat Yai, Songkhla, 90110 Thailand*

[3] *Department of Industrial Engineering, Rajamangala University of Technology Srivijaya, Mueang, Songkhla, 90000 Thailand*

Received: 9 September 2023; Revised: 27 December 2023; Accepted: 11 January 2024

Abstract

Railroad tracks are considered the main component of the rail system. As a maintenance guide, track condition inspection is necessary, especially for urban or high-speed railways where material deformation must always be detected to prevent unexpected failure. This paper examined the railway turnout, which consists of several vital components that allow trains to change direction. The nose area is made of high manganese steel and has an austenitic structure, unlike a rail track with a pearlitic structure. The microstructure and work hardening mechanism have been studied. The hardness of pearlitic rail steel increases when the lamellar spacing is more refined, with the maximum hardness found near the top surface. In the field, the austenitic structure has an original hardness of about 200 HV and increases up to 600 HV after service due to the twin mechanism. Ultrasonic testing was investigated for possibility of flaw detection in the rail materials, both in the lab and in the field.

Keywords: railway turnout, ultrasonic technique, work hardening mechanism, hadfield steel, R260 rail steel

1. Introduction

A standard turnout consists of several parts. This type of turnout is commonly used in Thai railway tracks. Cast manganese steel, known as "Hadfield," was used to construct the area known as the "Nose" instead of the standard rail around 7-8 years ago, due to its high toughness and work-hardening rate ranging from 180-210 HB to over 400 HB (Hodgson, 1993). The railhead at the turnout is subject to significant dynamic impact stresses as well as compressive rolling and sliding challenges. Compared to the standard rails, this section of the track is under a higher load (Kongpuang *et al.*, 2022). Hadfield steel must thus be utilized because of its superior mechanical properties. The total strength of Hadfield steel, which has a high work-hardening rate, is enhanced by the presence of carbides (Dastur & Leslie, 1981; Ghasri-Khouzani & McDermid, 2019). The R260 steel grade is commonly used to produce the standard grade rails. The pro-eutectoid ferrite forms at the grain boundaries in this steel grade, which has a nearly entirely pearlitic microstructure, while Hadfield steel used for crossings has an austenite-grain matrix containing 11-15 in wt % Mn, with 0.8-1.25 in wt % C (Curiel-Reyna *et al.*, 2007). Mn is an austenite stabilizer, allowing the face-centred cubic austenitic structure to stay stable at ambient temperature. Typically, the austenitic structure has difficulty with a grain structure that may quickly transition into a martensite structure.

♣Peer-reviewed paper selected from the 10th International Conference on Engineering and Technology
*Corresponding author
Email address: kmanwika@eng.psu.ac.th

Several papers have looked into the strengthening mechanisms of the two types of steel. Wear rates dropped with increasing hardness, lamellar spacing had an important effect on hardness, and pearlitic rail steel grade R260 was found to have a lower interlamellar gap. Also, harder steel had reduced or finer spacing, enhancing hardness (Lee & Polycarpou, 2005). Cleanliness improvements, inter-lamellar spacing reductions, and thick cementite lamellas can all potentially increase wear resistance (Olivares, Garcia, DeArdo, Kalay, & Hernández, 2011). Additionally, fine pearlite's increased plastic flow and fracture strain result in higher wear resistance (Korbel & Bochniak, 2017). Instability in the plastic flow of materials as a result of deformation twinning and interactions between stacking faults and dislocations enable Hadfield steel to undergo work-hardening in a short time (Hodgson, 1993). The increase in hardness would be to approximately three times that of the initial substance (Dhar *et al.*, 2019).

The most effective method for detecting cracks is ultrasonic testing (UT), which is not suitable for finding surface flaws until they propagate further inside (Kenderian, Berndt, Green Jr, & Djordjevic, 2003; Magel, Mutton, Ekberg, & Kapoor, 2016). At high speeds, particularly near the rail foot, surface flaws more minor than 4 mm may be overlooked as internal challenges (Ph Papaelias, Roberts, & Davis, 2008).

Therefore, this study focuses on studying the work hardening mechanism of Thai railway steel in the turnout area, associated with microstructure and hardness, allowing for early detection and prevention of potential failures. The findings from ultrasonic inspections will be crucial in informing maintenance schedules and strategies, ensuring the longevity and safety of the Thai railway system.

2. Materials and Methods

2.1 Materials

A standard turnout consists of several parts, as shown in Figure 1. In addition to the nose area, which is made of Hadfield steel with an austenitic structure, the other rails are pearlitic rail steel. This research prepared a plate of cast manganese steel procured from manufacturing to study the work-hardening mechanism. The R260 rail steel samples were extracted from the head of a used rail section. Optical Emission Spectroscopy (OES) was used to determine the elemental compositions of sample materials.

The chemical compositions of the rail steel R260 (EN54E1) and the Hadfield steel plate are shown in Table 1.

To study work hardening, the area where the sample is subjected to the wheel contact point versus the non-wheel contact area were compared. The contact position of wheels on rails is shown in Figure 2.

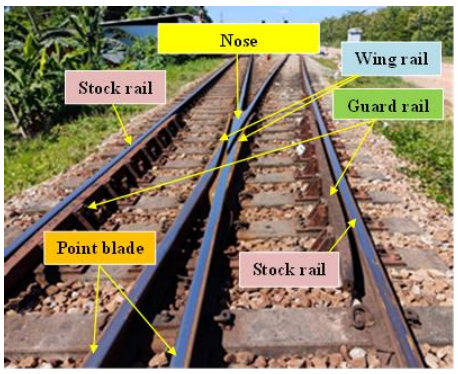

Figure 1. Standard turnout at Bangsaphanyai railway station (Kongpuang, 2022)

2.2 Metallography

Metallographic samples were cut off using a Struers Labotom-5 and mounted on Bakelite using a Struers CitoPress-1. The samples were ground and polished using Bainpol-VT before being etched to reveal the microstructure by using 2% Nital on R260 rail steel for 5 seconds and 10ml HNO_3 + 20ml HCl + 30ml water on Hadfield steel for 7 seconds. The microstructure of the metallographic samples was evaluated using an SEM-Quanta 400.

Table 1. Chemical compositions of the Hadfield steel and standard rail steel R260 (in weight %)

Material	Chemical composition (% wt)							
	C	Si	Mn	P	S	Cr	Ni	Al
R260	0.78	0.31	0.75	0.103	0.014	0.038	-	-
Hadfield steel	1.29	0.68	14.03	0.09	0.013	1.70	0.30	0.041

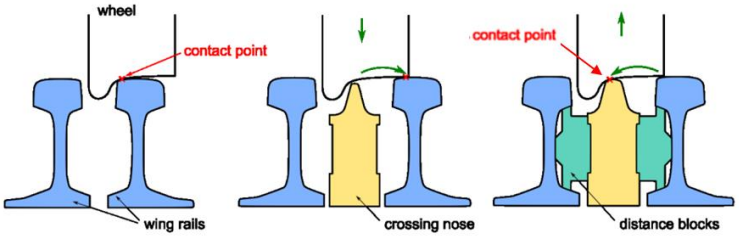

Figure 2. Transition of the wheel from the wing rail to the crossing nose (Ossberger, Pletz, Eck, Daves, & Ossberger, 2013)

2.3 Work-hardening of Hadfield steel

To simulate the changes in hardness, an increasing mechanism in Hadfield steel was experimented with, repeatedly hitting the specimen using a pounding hammer and checking the hardness using the Leeb Hardness tester HT-1000A. The test is stopped when the surface hardness is close to the maximum surface hardness measured on site. Then, the sample is taken for cross-sectioning to examine the microstructure and measure its hardness profile.

2.4 Hardness testing

In the laboratory, a microhardness Vicker tester MMT-X7B (with measurement unit HV) was used to measure R260 rail steel and Hadfield steel along the cross-section from the top surface down to the bottom, to compare the hardness profiles from the most affected impact area to the base metal with no impact. On-site measurements were done at the Hat Yai railway junction using Leeb Hardness tester HT-1000A at the turnout area. R260 rail steel was measured for hardness at the top of the rail and the curve of the rail head where the wheels contact, and Hadfield steel was measured for hardness across the entire nose area, to see differences in hardness by position.

2.5 Ultrasonic testing

Inspection of defects in railway steel using a conventional ultrasonic technique was tested with the Ultrasonic Flaw Detector KARL DEUSCH model Digital-ECHOGRAPH Serial Number 44371 with a probe having a 45-degree angle, in the turnout area. The graph is a scattering peak of the reflection of the ultrasonic wave signal that contacts defects in the material.

3. Results and Discussion

3.1 Work-hardening of pearlitic structures

The R260 rail steel sample shows a two-phased lamellar structure composed of alternating α-ferrite and cementite (Fe_3C) layers. As the amount of pearlite in the matrix increases, the work-hardening rate of ferrite-pearlite steel increases linearly (Pickering, 1992). Figure 3 shows the microstructure of the R260 rail steel with an almost entirely pearlitic structure. In these SEM images ferrite is dark and carbide is light. The average lamellar spacing in area A is about 190.6 nm, and in area B it is about 120.5 nm. The lamellar spacings at the wheel contact point and at the non-contact point are shown in Figure 4. They correspond to the measured hardness that increases when the lamellar spacing is decreased.

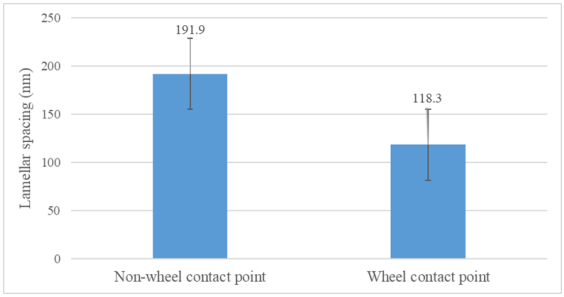

Figure 4. The lamellar spacings without and with wheel contact

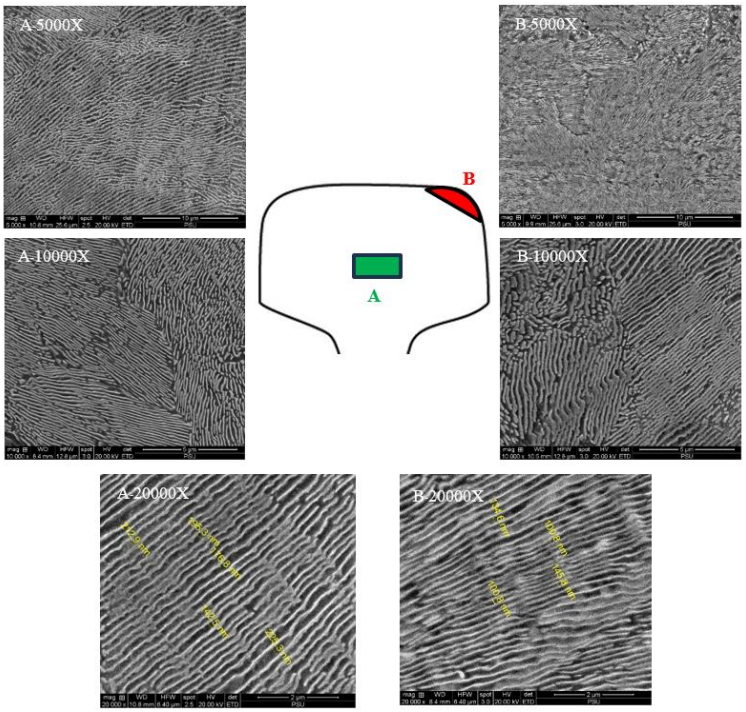

Figure 3. Microstructures in the R260 rail steel: (A) no wheel contact, and (B) wheel contact point (critical contact zone)

3.2 Work-hardening of austenitic structures

Hadfield manganese steel contains an austenite phase and carbide precipitate. As seen in Figure 5A, carbide precipitates appear at the grain boundary, lowering ductility and increasing hardness. As a result, intergranular cracking is simpler. Due to the high Mn content, Hadfield steel has an austenitic metastable microstructure. Repeated exposure to substantial loads causes the hardness to increase relative to the original structure, exhibiting outstanding wear resistance (Fei *et al.*, 2023; Kimura, Takemasa, & Honjo, 2011). According to Figure 5B-5E, the primary deformation processes in Hadfield manganese steel are dislocation and twinning (Kang, Zhang, Long, & Lv, 2014; Karaman, Sehitoglu, Gall, Chumlyakov, & Maier, 2000). The grain boundary twins deformation morphology is parallel straight lines passing through the grains and joining the grain boundaries, while the morphology of grain boundary carbides is either particle-like or short-rod morphology (Xu, Xia, Xiong, Lu, & Guo, 2023). The deeper layers are not subjected to significant work-hardening since the impact has little effect on the microstructure.

3.3 Hardness testing

3.3.1 Lab-based experiments

The lab-based hardness testing was with the Microvicker hardness test, over the cross-section areas on R260 rail steel and Hadfield steel. In the case of R260 rail steel with a pearlitic structure, the increased surface hardness corresponds to a reduced clearance in lamellar spacing, as explained in the microstructure section above. The initial R260 steel hardness is 260 HBN (equivalent to 275 HV) and can be increased up to 300HBN (equivalent to 320 HV) after use. The results of the hardness test along the cross-section of the rail head are shown in Figure 6. It was found that the maximum hardness at the top surface of the rail head was 350 HV, and the work hardening was about **7**mm deep from the surface.

A section from the Hadfield steel plate was laser cut to produce a sample with dimensions 250 mm x 20 mm x 15 mm (length x height x width) suitable for hammer testing. Hardness analysis was performed on Hadfield steel plates that had work hardening by subjecting to a load repeatedly with a hammer, to observe structural changes corresponding to increased hardness. Every 100 hits the sample was measured with a Leeb hardness instrument until the desired hardness of about 500-600 HV. Manual force was used to smash with a hammer for about 500 times. The results are shown in Figure 7. Hadfield manganese steel typically has a hardness of 200 HB (equivalent to 210 HV) when the solution is annealed and water quenched. This material can be strain-hardened to about 500 HB (equivalent to 530 HV). The work hardening is observed to extend up to a depth of around 10 mm from the running surface, and the wheel contact results in high deformation hardness of over 600 HV, approximately three times that of the as-received material. The crack path becomes wavy in this maximum hardness because most fractures pass through relatively soft grains in a direction free from the twins (Dhar *et al.*, 2019).

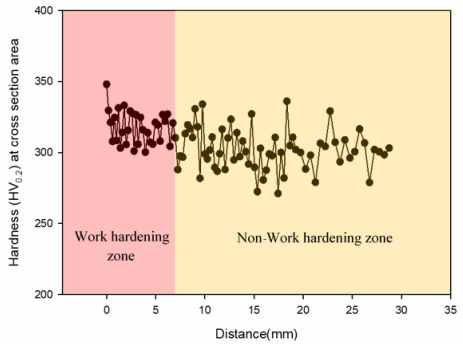

Figure 6. Hardness profile in a cross-section of R260 rail steel

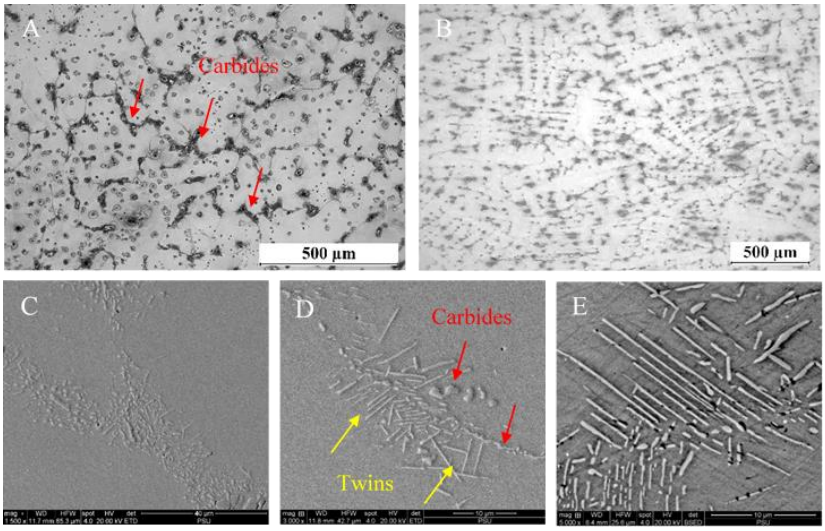

Figure 5. Microstructures in Hadfield steel: (A) Microstructure before work hardening shows carbide along grain boundaries, (B-E) microstructure after work hardening shows short-rod morphology of grain boundary carbides and parallel straight lines of grain boundary with twins deformation

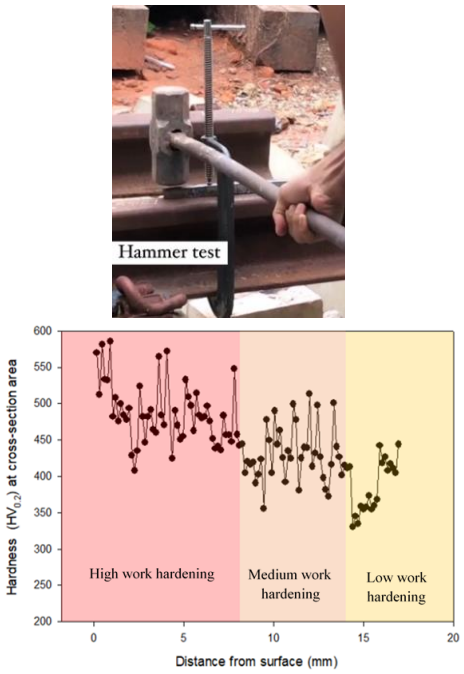

Figure 7. Hammer testing (top) and hardness profile in a cross-section of Hadfield steel after the test (bottom)

3.3.2 Field-based experiments

The hardness was measured on-site with a Leeb Hardness tester for the R260 rail steel top surface, as shown in Figure 8. The hardness can be divided into three areas: the area in contact with the wheel flange (a), the area in contact with the wheel tread (b), and the area in contact with the fieldside (c), which had average respective hardnesses of 300 HV, 295 HV, and 309 HV.

From measuring the hardness on site with the Leeb Hardness tester, the Hadfield steel crossing nose gave the three hardness ranges (a), (b), and (c), as shown in Figure 9. The test results gave the lowest 452 HV value in area (b), a hardness of 578 HV in area (c), and the highest 590 HV

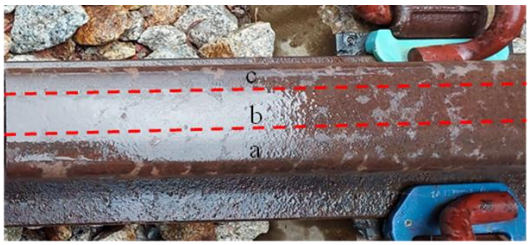

Figure 8. Field R260 rail steel with three hardness ranges in (a) area contacting wheel flange, (b) area contacting wheel tread, and (c) area on fieldside

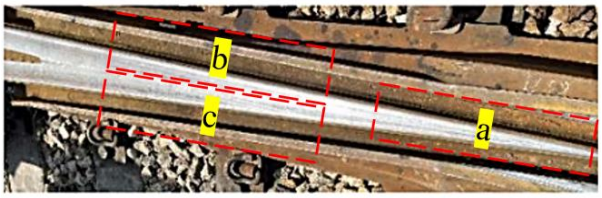

Figure 9. Crossing nose had three hardness ranges

hardness in area (a). It can be seen that the range with high hardness is located near the edge of the middle of the crossing nose. However, at the pointed end of the crossing nose at section a, the hardness range is less than that in other areas because this is an area that does not receive as much impact as the others. The maximum hardness measured on-site for R260 is 348 HV, while Hadfield steel reached 590 HV. The test results indicate that the hardness on site is approaching the maximum hardness of the material (BOZKURT, 2023; Dhar *et al.*, 2019). Therefore, there should be careful inspection to prevent damage to the material.

3.4 Flaw detection using ultrasonic testing

On-site inspection of defects in railway steel by using a conventional ultrasonic (UT) technique found defects in the switch and crossing area at the wing rail in both locations, as shown in Figure 10. The results obtained from

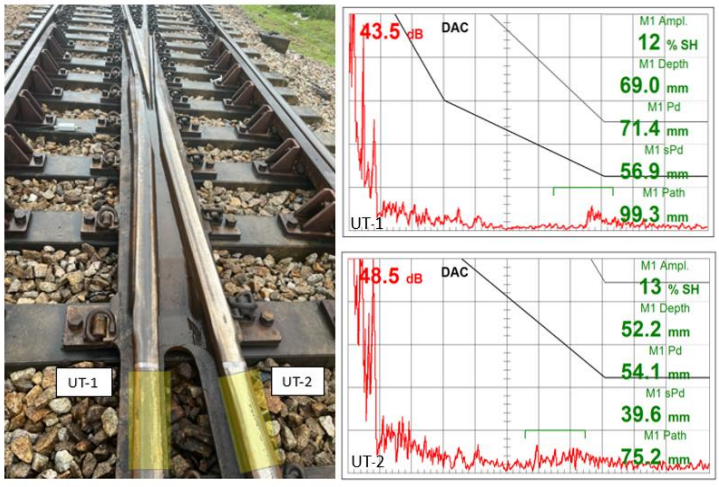

Figure 10. Location of inspection and test results for defects in rail steel at positions UT-1 and UT-2

inspection using the conventional ultrasonic technique are displayed as signal lines. The signal is reflected in a group of porosity distributed together, also called a group of cluster porosity. The size of the pore clusters found when compared with the standard values was within the acceptable range following an American Railway Engineering and Maintenance-of-Way Association (AREMA) manual standard in section 4.3, which recommends minimum performance guidelines for rail testing (Manual, 2006). No defects were found around the nose. It can be assumed in the two cases that there are no internal defects, or that UT cannot detect defects because the austenite structure has large grains, resulting in scattering of the beams from conventional UT (Bouda, Lebaili, & Benchaala, 2003).

4. Conclusions

Regarding the work-hardening of R260 rail steel, it can be concluded that decreasing inter-lamellar spacing similarly increases the work-hardening rate.

Work-hardening of Hadfield steel results from the twinning mechanism during plastic deformation in the metal.

The hardness values obtained from both lab and on-site testing showed that the surface area was close to the maximum hardness for the material after work hardening, so it is important to start monitoring the location for possible damage.

Conventional ultrasonic testing is effective for detecting defects in the pearlitic or fine-grained structure, but is unsuitable in austenitic or coarse structures due to beam scattering. Therefore, other techniques, such as Phased Array Ultrasonic Testing (PAUT) or Acoustic Emission Testing (AET), are more appropriate.

Acknowledgements

This research was supported by Faculty of Engineering, Academic year 2022-2023, Prince of Songkla University, Thailand and National Science, Research and Innovation Fund (NSRF). The authors are grateful to the Graduate School and the Department of Mining and Materials Engineering, Faculty of Engineering, Prince of Songkla University, and the Center of Excellence in Metal and Materials Engineering (CEMME) for the provision of facilities, equipment, and financial support for this project.

References

American Railway Engineering and Maintenance-of-Way Association. (2006). *Manual for railway engineering*. Lanham, MD: Author.

Bozkurt, F. (2023). Investigation of Tribological properties of head, web and foot sections of R260 Rail. *Demiryolu Mühendisliği*, *17*, 107-114.

Bouda, A. B., Lebaili, S., & Benchaala, A. (2003). Grain size influence on ultrasonic velocities and attenuation. *Ndt and E International*, *36*(1), 1-5.

Curiel-Reyna, E., Contreras, J., Rangel-Ortis, T., Herrera, A., Baños, L., Real, A. d., & Rodríguez, M. (2007). Effect of carbide precipitation on the structure and hardness in the heat-affected zone of Hadfield steel after post-cooling treatments. *Materials and Manufacturing Processes*, *23*(1), 14-20.

Dastur, Y. N., & Leslie, W. (1981). Mechanism of work hardening in Hadfield manganese steel. *Metallurgical Transactions A*, 12, 749-759.

Dhar, S., Danielsen, H. K., Fæster, S., Rasmussen, C., Zhang, Y., & Jensen, D. J. (2019). Crack formation within a Hadfield manganese steel crossing nose. *Wear*, *438*, 203049.

Fei, J., Zhou, G., Zhou, J., Zhou, X., Li, Z., Zuo, D., & Wu, R. (2023). Research on the effect of pearlite lamellar spacing on rolling contact wear behavior of U75V rail steel. *Metals*, *13*(2), 237.

Ghasri-Khouzani, M., & McDermid, J. (2019). Modeling the work hardening behavior of high-manganese steels. *Journal of Materials Engineering and Performance*, *28*, 1591-1600.

Hodgson, W. (1993). Rail metallurgy and processing. Paper presented at the Rail Quality and Maintenance for Modern Railway Operation: International Conference on Rail Quality and Maintenance for Modern Railway Operation Delft June 1992.

Kang, J., Zhang, F., Long, X., & Lv, B. (2014). Cyclic deformation and fatigue behaviors of Hadfield manganese steel. *Materials Science and Engineering*: *A*, *591*, 59-68.

Karaman, I., Sehitoglu, H., Gall, K., Chumlyakov, Y. I., & Maier, H. (2000). Deformation of single crystal Hadfield steel by twinning and slip. *Acta materialia*, *48*(6), 1345-1359.

Kenderian, S., Berndt, T. P., Green Jr, R. E., & Djordjevic, B. B. (2003). Ultrasonic monitoring of dislocations during fatigue of pearlitic rail steel. *Materials Science and Engineering*: *A*, *348*(1-2), 90-99.

Kimura, T., Takemasa, M., & Honjo, M. (2011). Development of SP3 rail with high wear resistance and rolling contact fatigue resistance for heavy haul railways. *JFE Technical Report*, *16*, 32-37.

Kongpuang, M., Culwick, R., Cheputeh, N., Marsh, A., Jantara Junior, V. L., Vallely, P., . . . Papaelias, M. (2022). Quantitative analysis of the structural health of railway turnouts using the acoustic emission technique. *Insight-Non-Destructive Testing and Condition Monitoring*, *64*(7), 398-403.

Kongpuang, M. (2022). *Reliability-base monitoring and maintenance of urban railway turnout using acoustic emission*. University of Birmingham, Birmingham, England.

Korbel, A., & Bochniak, W. (2017). Stratified plastic flow in metals. *International Journal of Mechanical Sciences*, *128*, 269-276.

Lee, K. M., & Polycarpou, A. A. (2005). Wear of conventional pearlitic and improved bainitic rail steels. *Wear*, *259*(1-6), 391-399.

Magel, E., Mutton, P., Ekberg, A., & Kapoor, A. (2016). Rolling contact fatigue, wear and broken rail derailments. *Wear*, *366*, 249-257.

Olivares, R. O., Garcia, C., DeArdo, A., Kalay, S., & Hernández, F. R. (2011). Advanced metallurgical alloy design and thermomechanical processing for rails steels for North American heavy haul use. *Wear*, *271*(1-2), 364-373.

Ossberger, U., Pletz, M., Eck, S., Daves, W., & Ossberger, H. (2013). Validation of a finite element crossing model using measurements at an instrumented turnout. Paper presented at the 10th International Heavy Haul Conference IHHA 2013.

Ph Papaelias, M., Roberts, C., & Davis, C. L. (2008). A review on non-destructive evaluation of rails: state-of-the-art and future development. *Proceedings of the Institution of Mechanical Engineers, Part F: Journal of Rail and Rapid Transit*, *222*(4), 367-384.

Pickering, F. (1992). *Bainite in steels*. Oxfordshire, England: Taylor and Francis.

Xu, Z., Xia, Z., Xiong, Y., Lu, J., & Guo, Z. (2023). Multiple morphologies and twin structure generated by a definite growth behavior of grain boundary M23C6 in tempered Fe–15Mn–3Al-0.7 C steel. *Journal of Materials Research and Technology*.